

Transfer Strategy for Near Infrared Analysis Model of Holocellulose and Lignin Based on Improved Slope/Bias Algorithm

Honghong Wang, Zhixin Xiong,* Yunchao Hu, Zhijian Liu, and Long Liang

Model transfer techniques in near infrared spectroscopy are important for avoiding duplicate modeling, sharing samples and data resources, and reducing the human and material consumption required for modeling. Use of the slope/bias correction algorithm (S/B) based on screening wavelengths with consistent and stable signals (SWCSS) for model transfer is a new strategy. To enable sharing of near infrared analysis models of pulp holocellulose and lignin content in two different types of spectroscopic instruments, a combined SWCSS-S/B algorithm was proposed. The stable and consistent wavelengths between the spectroscopic instruments screened by the SWCSS method reduced the differences between the instruments, thereby improving the universality and transmission accuracy of the S/B method. The SWCSS-S/B based model transfer method reduced the predicted standard deviation RMSEP of holocellulose and lignin contents of the samples measured on the target spectrometer of the from 5.4686 and 7.6823 to 1.2133 and 1.3494, respectively. This result showed a significant improvement in the transfer effect compared to the SWCSS and S/B correction results alone, and the prediction of holocellulose was better than that of the prediction effect of lignin. The method has fewer wavelength variables involved in model transfer, fast transfer speed, and high prediction accuracy, which provides a new solution for the wide application of NIR analytical models.

DOI: 10.15376/biores.17.4.6476-6489

Keywords: Near infrared spectroscopy; Holocellulose; Lignin; Stable and consistent wavelength; Slope/Bias algorithm; Model transfer

Contact information: College of Light Industry and Food Engineering, Nanjing Forestry University, Longpan Road 159, Nanjing 210037 China; *Corresponding author: Leo_xzx@njfu.edu.cn

INTRODUCTION

Holocellulose (including cellulose and hemicellulose) and lignin are the main components of wood. They are closely related to other wood properties as well as to the processing and utilization of wood. In the paper industry, the holocellulose content is closely related to the pulp yield and pulp quality; the lignin content is an important basis for the development of cooking and bleaching conditions (Haque *et al.* 2019). Near infrared spectroscopy (NIRS) is widely used in pharmaceutical, food, petrochemical, agricultural products, feed, tobacco, and other industries because it does not require chemical methods for sample pre-treatment and has the advantages of being green, efficient, non-destructive, and easy to implement for online use (Pažitný *et al.* 2011; Yu *et al.* 2021; Cao *et al.* 2022). However, in the practical application of spectroscopic measurements, a model built on one instrument (master instrument) is applied to another instrument (target instrument) with a large deviation or even unusable problem. Such problems are generally referred to as model

failure problems, and model transfer methods are generally used to solve such problems. Model transfer can effectively avoid duplicate modeling and realize the sharing of sample and data resources; it is important for the promotion of NIR spectroscopy applications (Wang *et al.* 2019; Feudale *et al.* 2002).

The model transfer algorithm used can be divided into methods with standard samples and methods without standard samples according to whether one-to-one correspondence of standard spectra should be collected on all instruments (Zhang *et al.* 2020). The model transfer algorithm with standard samples must take a certain number of samples to form a standard sample set, such as Slope/Bias (S/B) (Du *et al.* 2011; Zhao *et al.* 2019), direct standardization (DS) (Parrott *et al.* 2022) and piecewise direct standardization (PDS) (Bergman *et al.* 2006; Peng *et al.* 2011). Commonly used model transfer methods without standards include signal processing methods, such as wavelet transform (WT) (Bin *et al.* 2017; Abasi *et al.* 2019), orthogonal projection (Poerio and Brown 2018), and linear model correction (Liu *et al.* 2016). Ni *et al.* (2019) proposed a NIR model transfer method without standards based on the wavelength of stable consistent spectral signal (SWCSS) by screening out the wavelengths with stable consistent spectral signal between instruments and establishing a correction model for model transfer. Such an approach is better for model transfer prediction between spectrometers of the same type and with small differences, but it is not suitable for model transfer between different types of spectrometers because it does not use transformation sets for spectrum or model correction. Li *et al.* (2018) conducted a model transfer study for two indexes of edible oil, acid value and peroxide value, using the S/B algorithm combined with partial least square regression (PLSR) model established on a master spectroscopy instrument. The results show that the model prediction results were improved to different degrees after the S/B algorithm transfer, but the model prediction results after the S/B algorithm transfer still had a big gap with the ideal results. In previous studies (Liu *et al.* 2019a,b), the S/B method was applied to the transfer of pulp wood lignin NIR spectroscopy models between two different types of convenient NIR spectrometers, and the model transfer effects of the S/B, DS and canonical correlation analysis (CCA) algorithms (Li *et al.* 2022) were compared. The S/B algorithm based on linear correction among these three algorithms could not obtain the model transfer effect to meet the accuracy requirements. The applicability is low when using SWCSS and S/B algorithms alone for model transfer, and the model transfer between spectrometers with large differences is poor.

In the present study, a model transfer method of SWCSS combined with S/B algorithm is proposed. The method reduces the differences between different NIR spectrometers by screening out the consistent wavelengths with small differences between instruments and improves the transfer accuracy and applicability of S/B algorithm, which makes up for the shortcomings of using SWCSS and S/B algorithm alone. Using 82 wood flour samples, the transfer effect of the holocellulose and lignin content models based on the SWCSS-S/B method was investigated between two IAS NIR spectrometers of different types; it was compared with the transfer effect of the SWCSS, S/B and PDS and DS algorithms alone. The aim was to improve the robustness and sharing of NIR correction models with a view to providing methodological references for the application of NIR spectroscopy detection techniques in the determination of the integrated holocellulose and lignin contents of pulpwood.

PRINCIPLE AND ALGORITHM

Screening Wavelengths with Consistent and Stable Signals

The standard deviations of the following two spectra were calculated based on the spectral information of the sample.

Standard deviation of precision detection spectra

The standard deviation SDPDS of the spectrum of the same sample taken n times in succession on the master spectrometer was calculated using Eq. 1,

$$\text{SDPDS}(j) = \sqrt{\frac{\sum_{i=1}^n (X_{ij} - \bar{X}_j)^2}{n-1}} \quad (1)$$

where X_{ij} is the spectral information of the j^{th} wavelength of the measured sample at the i^{th} acquisition, and n is the number of acquisitions. \bar{X}_j is the average value of the spectral information of the j^{th} wavelength. SDPDS reflects the size of the variation of the instrument noise and measurement error within a short period of time. The smaller the SDPDS, indicates a more stable spectral signal of that wavelength.

Standard deviation of difference spectra between master and target Instruments

SDDSI reflects the size of the variation of the master and target difference spectra. This quantity was calculated using Eq. 2,

$$\text{SDDSI}(j) = \sqrt{\frac{\sum_{i=1}^m (A_{ij} - \bar{A}_j)^2}{m-1}} \quad (2)$$

where m is the number of samples, M_{ij} and S_{ij} are the spectral response values of sample i measured by the master and target at wavelength j , separately, and $A_{ij} = M_{ij} - S_{ij}$ is the difference spectrum between the two spectroscopic instruments. A smaller SDDSI $_j$, demonstrates a smaller difference between the spectral signals of these two spectroscopic instruments at wavelength j , suggesting that the wavelength is more stable.

Screening and optimization of stable and consistent wavelengths

A certain number of representative samples are selected by Kennard-Stone (Zhang *et al.* 2017; Sadergaski *et al.* 2022) algorithm, and then, the SDDSI $_j$ and SDPDS $_j$ at wavelength j are calculated according to Eqs. 1 and 2 above. The ratio of these two is defined as the consistency parameter,

$$b_j = \frac{\text{SDDSI}_j}{\text{SDPDS}_j} \quad (j=1, 2, 3, \dots, n) \quad (3)$$

where n is the number of wavelengths. Usually, SDDSI $_j$ is larger than SDPDS $_j$. The closer b_j is to 1, the smaller the spectral difference between instruments at that wavelength and the better the spectral signal stability. In practical applications the b value is set to filter out wavelengths with SDDSI $_j$ /SDPDS $_j < b$ for the wavelength. In addition, the set of wavelengths between the master and target instruments screened according to the above method is noted as U_c , from which the wavelengths with large SDPDS values are excluded to arrive at the wavelength set with better stability U_{sc} .

Slope /Bias Correction Algorithm

The S/B algorithm is a standardized correction method for model prediction results. The calibration model built on the master machine is used to predict the predicted values X_m and X_s of the spectral matrix X_m measured on the master and target machines for the specimen set to obtain the spectra y_m and y_s , respectively. The parameters y_m and y_s are assumed to have the following relationship,

$$y_s = \text{Slope}y_m + \text{Bias} \quad (4)$$

where Slope is the slope of the linear equation and Bias is the intercept of the linear equation, which can be calculated by Least Square (LS). For the unknown sample spectral matrix $X_{s,un}$ measured on the target instrument; first, $y_{s,un}$ is predicted by the calibration model built on the master instrument, and then, the passed prediction $y_{s,tr}$ can be found by the following equation,

$$y_{s,tr} = \text{Slope}y_{s,un} + \text{Bias} \quad (5)$$

where $y_{s,un}$ is the predicted value of the unknown sample and $y_{s,tr}$ is the predicted value of the unknown sample after passing.

EXPERIMENTAL

Sample Preparation and Analysis of Holocellulose and Lignin Content

A total of 82 log samples were cut into chips and ground, and the wood flour samples with particle sizes of 0.250 to 0.425 mm (40 to 60 mesh) were selected to determine their holocellulose and lignin contents according to GB/T 2677.8 (1994). The results of are shown in Table 1.

Table 1. Statistical Table of the Content of Holocellulose and Lignin in Wood

Component	Number of samples	Minimum value	Maximum value	Average value	Standard deviation
Holocellulose	82	66.08	86.28	76.14	5.97
Lignin	82	14.82	34.20	26.43	5.42

Instrumentation and Spectral Acquisition

The experimental instrument adopts two IAS series portable spectrometers from the same company (Wuxi Intelligent Analysis Service Co. Ltd, Wuxi, China). The core components of the instruments are digital micromirror device grating spectrometers based on micro-electromechanical systems, with a wavelength range of 900 to 1700 nm and a resolution of 10 nm. One of them is an IAS-5000 type, marked as 5000B (master instrument), using a down-illuminated 5W halogen tungsten light source; the other is an IAS-2000 type, marked as 2000 (target instrument), with an up-illuminated 10W tungsten-halogen lamp light source. The two types of instruments are shown in Fig. 1. When collecting the sample spectrum, the sample was put into the measuring cup and flattened with a 50 g weight to make it evenly distributed, and each sample was repeatedly loaded three times to take the average spectrum. The number of spectral scans was 50, and for each sample measured, the residual wood powder in the sample cup was removed with a brush to avoid affecting the accuracy of subsequent sample spectra acquisition. The spectra

of 82 wood powder samples were collected by the above method on two types of instruments under the same environmental conditions, respectively. The collected spectral data were preprocessed using Standard Normal Variate Transformation (SNV) (Kang *et al.* 2022; Maraphum *et al.* 2022) to eliminate the interference of surface scattering and light range variation of wood samples on the NIR diffuse reflectance spectra for the subsequent wavelength screening and modeling process.

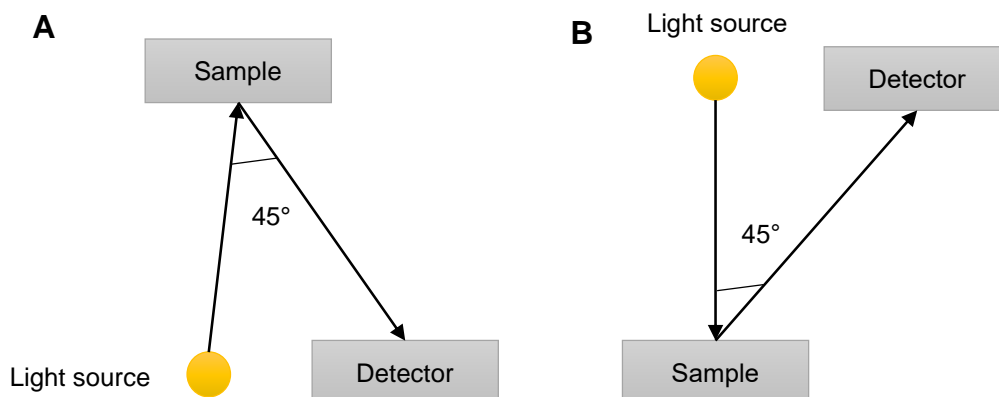


Fig. 1. Diagram of two irradiation modes, (A) bottom-up irradiation (B) top-down irradiation

Sample Set Division

Aiming at the spectral data of 82 samples used in this paper, after extracting 3 principal components by PCA algorithm, the Kennard-Stone method was used to divide 56 calibration sets and 26 prediction set samples. The calibration set and prediction set samples of the master and target instruments corresponded to each other. The distribution of holocellulose and lignin contents of pulpwood is shown in Table 2.

Table 2. Holocellulose and Lignin Contents of Wood Powder in Correction Set and Prediction Set

Component	Sample set Division	Number of Samples	Minimum Value	Maximum Value	Average Value	Standard Deviation
Holocellulose	Calibration set	56	66.08	86.28	77.18	5.70
	Prediction set	26	66.22	81.70	73.89	6.03
Lignin	Calibration set	56	14.82	34.20	25.45	5.32
	Prediction set	26	18.20	33.84	28.55	5.11

Modeling and Model Evaluation Methods

The partial least squares regression (PLSR) method was used for modeling (Moreira *et al.* 2015). The number of latent variables was set in the range of 2-14, and determined by leave-one-out cross validation (Zhang *et al.* 2022). The calibration model and model transfer effect established using PLSR and the model prediction ability were evaluated comprehensively by the coefficient of determination (R^2), root-mean standard error for cross-validation (RMSECV), root mean square error of prediction (RMSEP), and relative predictive determinant (RPD) between the predicted and true values of the samples in order to establish the optimal prediction model. Among them, the closer the coefficient of determination R^2 is to 1, the better the regression or prediction result of the model, and if R^2 is small, it indicates a very poor fit. Smaller RMSECV and RMSEP values indicate a better model effect (Zhang *et al.* 2019; Fatchurrahman *et al.* 2021); RPD is used to verify

the stability and predictive ability of the model. The model is good when $RPD > 2.5$, average but usable when RPD is 2 to 2.5, and unusable when $RPD < 2$ (Hao *et al.* 2022).

RESULTS AND DISCUSSION

Screening for Stable and Consistent Wavelengths

The number of representative samples K selected from the master instrument samples by Kennard-Stone method was 5, 10, 15, and 20, and these representative samples were used to screen the wavelength U_c with consistent and stable spectral signals between the master and the target instruments. The wavelength set U_c of the master and the target was screened by SWCSS method according to the number of different representative samples K . Using the wavelength set U_c to build a master model to predict the variation of RMSEP with consistency parameter b value for the prediction set samples of the target (as shown in Fig. 2). During the experiment, the wavelength set U_c was screened by setting b to be taken from 1 to 10, but when $b=1$ the number of wavelengths selected according to the SWCSS algorithm step was 0, and the model could not be built. Therefore, U_c was screened by setting consistency the parameter b to take 2 to 10. The suitable b value was selected by predicting the minimum RMSEP of the target samples with the master PLSR model for both the integrated holocellulose and lignin indexes, respectively. From Fig. 2, it can be seen that the master model established by the U_c wavelength set screened by selecting 5 representative samples for holocellulose and setting $b=7$ had the best prediction effect on the target samples. The wavelength set screened by the SWCSS method based on holocellulose was denoted as U_{ch} , and it contained 449 characteristic wavelengths with consistent and stable signals. For lignin, 20 representative samples were selected, and the U_c wavelength set with $b=8$ had the best prediction. The wavelength set screened by the SWCSS method based on lignin was denoted as U_{cl} , which contained 659 consistent and stable characteristic wavelengths. Since there were no wavelength points with excessive SDPDS values in U_{ch} and U_{cl} , the wavelength sets U_{sch} and U_{scl} screened by the SWCSS method based on holocellulose and lignin have 449 and 659 consistent wavelengths, respectively, and their distributions are shown in Fig. 3.

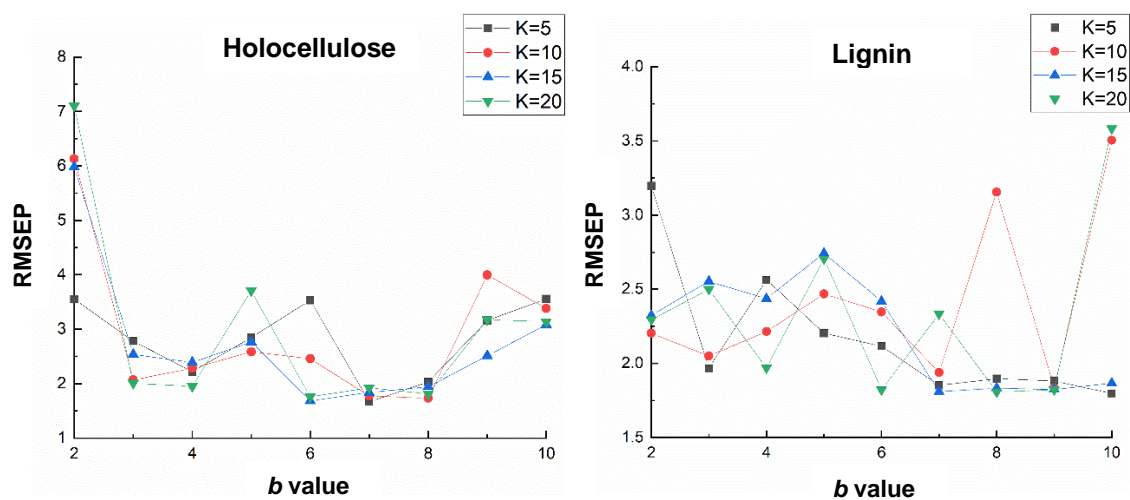


Fig. 2. Prediction of RMSEP of target instrument samples with the value of consistency parameter b based on a master instrument holocellulose and lignin model built on stable consistency wavelengths

As shown in Fig. 3, the wavelength points $Usch$ and $Uscl$ selected by the SWCSS method based on the two indicators of holocellulose and lignin were mainly located in the region where the standard deviation SDDSI between the master and the target was small, while in the regions with large differences such as 900 to 965, 1056 to 1058, 1064 to 1068, 1072 to 1079, 1630, 1636, 1640 to 1641 and 1644 to 1700 nm, none of them could pass the SWCSS screening.

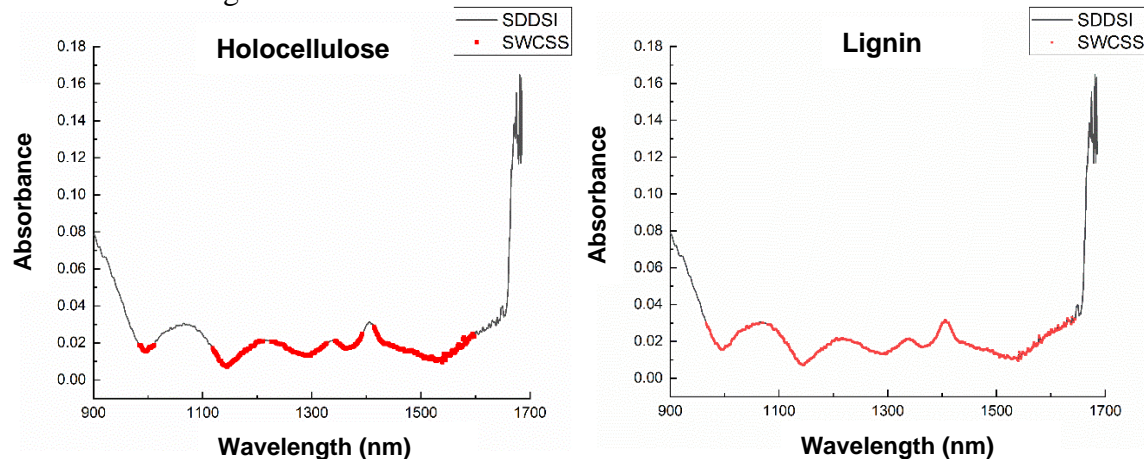


Fig. 3. Location distribution of $Usch$ and $Uscl$ of consistent wavelength sets of holocellulose and lignin screened by SWCSS method

As a further analysis, the PCA method (Ferrara *et al.* 2022; Hasan *et al.* 2022) was used in this study to characterize the differences in spectra between NIR spectroscopy instruments. The PCA scores of 56 calibration set samples for the full spectra of the 2 instruments (master and target) and the wavelength set screened based on the SWCSS method were calculated, and the results are shown in Fig. 4(A) and Fig. 4(B), separately.

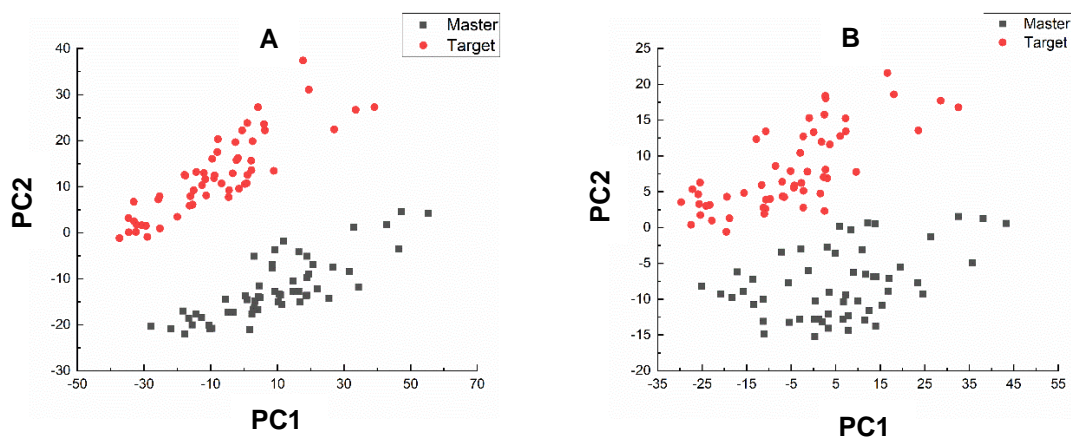


Fig. 4. Principal Components 2D Score Plot of 2 instruments

As can be seen in Fig. 4(A), the differences between the master and target instruments characterized using the full spectrum PCA scores were significant because the target and master were different types of instruments, and their irradiation directions, light source power and assembly processes were different. The average martensite distance between the master and the target was 2.3679 calculated from the sample spectra. As can be seen in Figs. 3 and 4(B), the wavelengths screened by the SWCSS method were mainly located in the wavelength region where the standard deviation SDDSI of the master and

target instruments is small, indicating that the selected wavelengths have good consistency and can be effectively reduced. The difference between the two spectrometers, the average Mahalanobis distance between the master and the target was 0.9585. Therefore, further correction using the S/B method based on the consistent wavelengths screened by the SWCSS method may enable the model built on the master instrument to achieve higher prediction accuracy on the target instrument.

Results and Analysis of Model Transfer of Holocellulose and Lignin in Pulpwood Synthesis

Pre-transfer modeling and prediction of holocellulose and lignin models

In this study, 56 calibration set samples were used to build PLSR models for holocellulose and lignin contents of the master instrument based on SWCSS and full-spectrum wavelengths, respectively. The appropriate number of latent variables (LV) was selected by the leave-one-out cross-validation method (Zhang *et al.* 2022), and the results are shown in Table 3.

Table 3. Prediction Results of Master and Target Prediction Sets by Master instrument Calibration Model before Model Transfer

Component	Methods	LV	Correction set			Prediction set		
			R ²	RPD	RMSEP	R ²	RPD	RMSEP
Holocellulose	Full Spectrum	10	0.9641	5.2796	1.1202	0.9598	4.9847	1.1335
	SWCSS	9	0.9662	5.4393	1.0382	0.9593	4.9546	1.1937
Lignin	Full Spectrum	10	0.9644	5.3000	0.9945	0.9475	4.3638	1.1490
	SWCSS	8	0.9681	5.5989	0.9412	0.9339	3.8898	1.2890

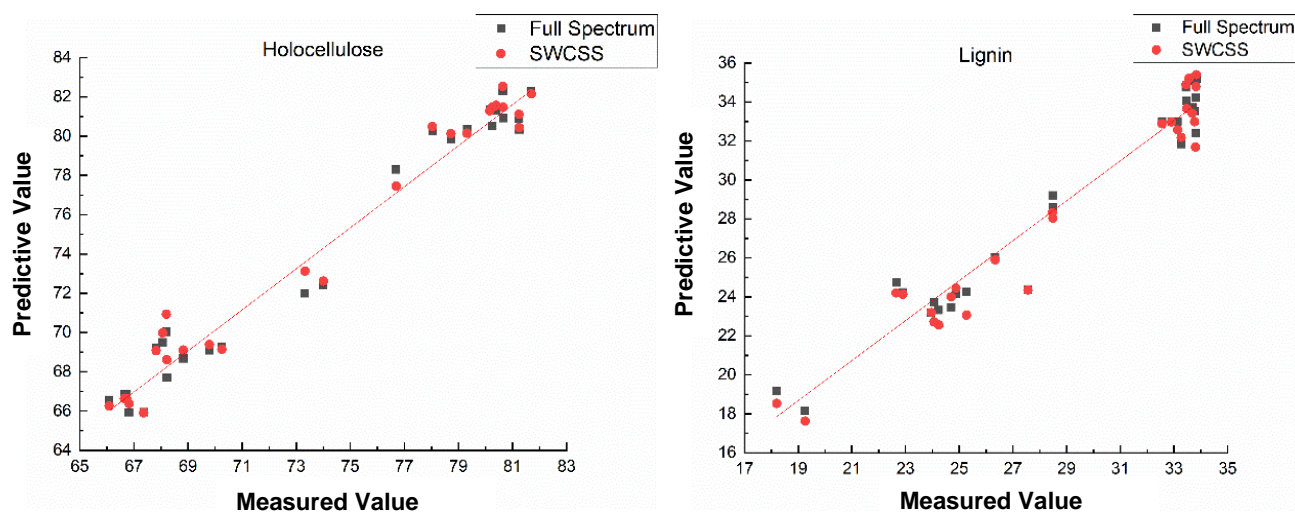


Fig. 5. Correlation diagram between the measured value and the predicted value of the master instrument sample predicted by the master instrument model established based on different wavelength sets

Figure 5 shows the correlation plots between the measured and predicted values of holocellulose and lignin contents for the 2 master calibration models in Table 3, which contains the fitted straight lines of the one-element regression between the predicted set of

holocellulose and lignin contents and the actual contents of the master samples from the master full-spectrum model analysis before model transfer. As shown in Table 3 and Fig. 5, the RPDs of the predicted results of the master instrument calibration models based on the above different wavelength sets are all greater than 3.8. The points corresponding to the predicted values are all roughly distributed around the fitted straight lines in Fig. 5, and the offset is small. This shows that the master instrument models established by the above different wavelength selection methods can meet the requirements of practical applications.

Model transfer results and analysis

Both the full-spectrum-based S/B and SWCSS-S/B algorithms are standard samples algorithms, which require the selection of transfer set samples in the scale-sets of the master and the target, respectively. Therefore, the Kennard-Stone algorithm was used to take 5, 10, 15, 20, 25, 30, 35, and 40 samples in the specimen sets of the master and target instruments respectively as the transfer sets for model transfer. The relationship between the number of samples in the transfer set and the RMSEP is shown in Fig. 6. The best prediction of holocellulose and lignin was achieved by selecting 5 and 20 transfer set samples respectively in the model transfer process using S/B algorithm. The best prediction of holocellulose and lignin was achieved by selecting 25 and 30 transfer set samples respectively in the model transfer process between the master and target instruments using the SWCSS-S/B algorithm.

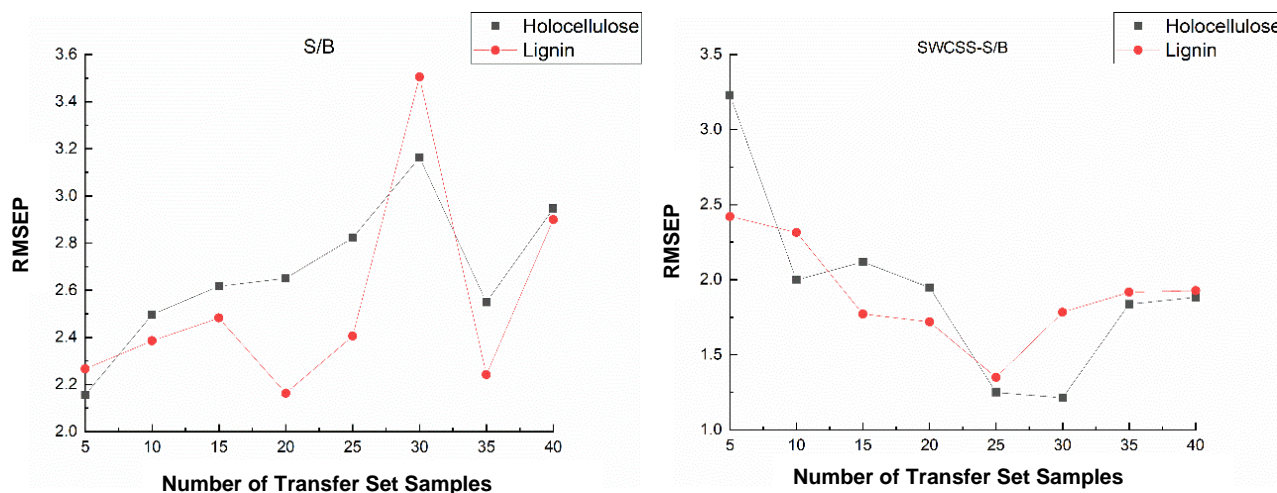


Fig. 6. Master's holocellulose and lignin models predict target's RMSEP as a function of the number of samples in the transform set

To further analyze the transfer effect of the SWCSS-S/B algorithm proposed in this study, the optimal number of transfer set samples selected by the S/B and SWCSS-S/B algorithms were used for model transfer of 26 prediction set samples from the target instrument, separately, and compared with the SWCSS, S/B, PDS, and DS algorithms alone. Results are shown in Table 4. There was a large prediction error when the full-spectrum model of the master was used to analyze the target measurement samples directly, and the RPDs of the predicted holocellulose and lignin were 1.0815 and 0.6527, respectively, which cannot meet the practical application requirements. The prediction effect of the PDS and S/B algorithms alone for the target instrument was somewhat improved relative to that before model transfer, but the RPDs of both algorithms were less than 2.5, and the prediction accuracy was not high. In contrast, the transfer effect of using

the SWCSS-S/B algorithm was significantly improved, and the RPDs of predicting the target instrument holocellulose and lignin were 4.8746 and 3.7157, respectively, which were close to the transfer results of the DS algorithm. This indicates that the SWCSS-S/B method had better stability and transfer effect than the SWCSS and S/B algorithms alone. This is because the consistent wavelengths screened by the SWCSS method are located in the wavelength region with small differences between instruments, which greatly reduces the differences between the master and target instruments, and then the S/B algorithm is used to further correct the systematic errors that still exist after the SWCSS correction can achieve better model transfer results. Although the transfer effect of the SWCSS-S/B method is slightly inferior to that of the DS algorithm, in practical applications the former is involved in holocellulose and lignin model transfer at 449 and 659 wavelengths, respectively, with fewer wavelength variables and faster computing speed, which is convenient for practical applications.

Table 4. Transfer Effect of Different Model Transfer Methods

Component	Methods	Master			Target		
		R ²	RPD	RMSEP	R ²	RPD	RMSEP
Holocellulose	Full spectrum	0.9598	4.9847	1.1335	0.1450	1.0815	5.4686
	PDS	-	-	-	0.8058	2.2695	2.3030
	DS	-	-	-	0.9645	5.3051	1.1148
	S/B	-	-	-	0.8042	2.2599	2.6169
	SWCSS	0.9593	4.9546	1.1937	0.9205	3.5475	1.6671
	SWCSS-S/B	-	-	-	0.9579	4.8746	1.2133
Lignin	Full spectrum	0.9475	4.3638	1.1490	-1.3475	0.6527	7.6823
	PDS	-	-	-	0.8050	2.2647	2.2140
	DS	-	-	-	0.9481	4.3914	1.1418
	S/B	-	-	-	0.7549	2.0199	2.4825
	SWCSS	0.9339	3.8898	1.2890	0.8700	2.7733	1.8079
	SWCSS-S/B	-	-	-	0.9276	3.7157	1.3494

Figures 7 and 8 are the correlation diagrams and their distribution diagrams of the measured and predicted values of the holocellulose and lignin contents of the target instrument before and after transfer using different models such as DS, PDS, SWCSS, and S/B independently and in combination. As a reference, the figure also draws a single regression fitting straight line between the predicted and actual content of holocellulose and lignin in the master instrument samples analyzed by the master instrument full spectrum model. As can be seen in Figs. 7 and 8, before the model transfer, the master instrument model had the worst prediction results for the holocellulose and lignin content of the target instrument samples, and the longitudinal offset was also the largest. The transfer results of the PDS and S/B methods were poor, the predicted values were obviously distributed on both sides of the fitted line in a wider range, and the longitudinal offset was large (Fig. 7(A), Fig. 7(B) and Fig. 8(A), Fig. 8(B)). However, the prediction errors of the master instrument holocellulose and lignin models established by the SWCSS and SWCSS-S/B methods when applied to the target instrument samples were reduced, and the predicted values were roughly distributed in a narrow range along the fitted straight line.

The offset was small, and most of the predicted values of the master instrument model corrected by the SWCSS-S/B method for the target were closer to the fitted straight line. This further indicates that the model prediction statistical error after the transfer of the SWCSS-S/B method was smaller, and the prediction effect of holocellulose was better than that of lignin.

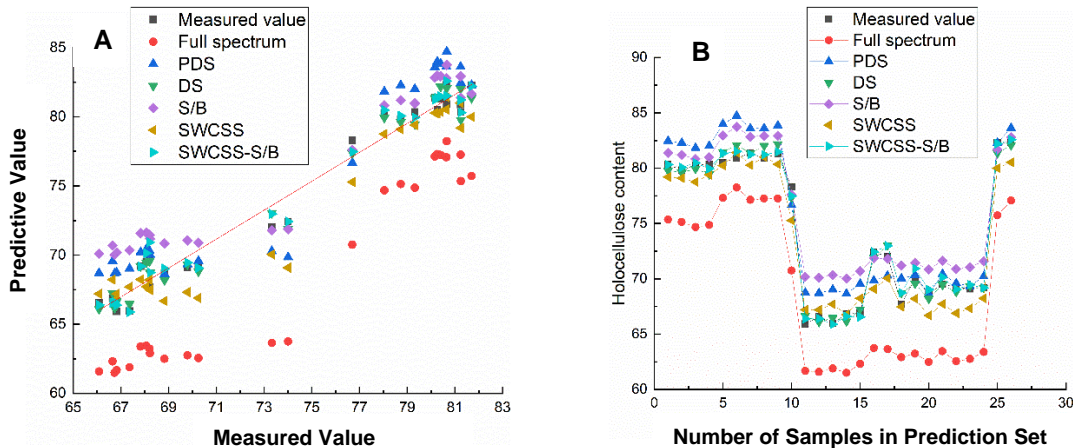


Fig. 7. Correlation diagram and distribution diagram of the measured and predicted values of the predicted concentration of holocellulose content

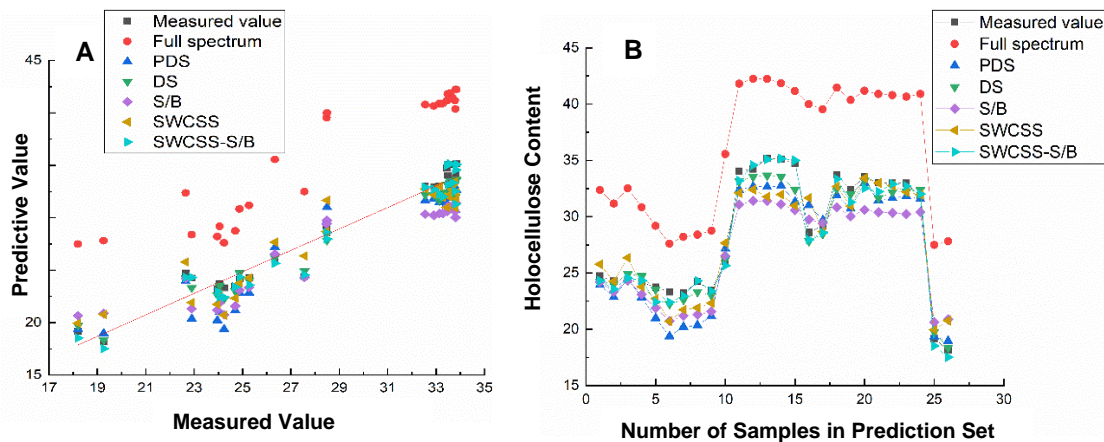


Fig. 8. Correlation diagram and distribution diagram of the measured and predicted lignin content in the predicted concentration

CONCLUSIONS

1. The research showed that the SWCSS-S/B method achieved good results in the transfer process of the model of pulp wood holocellulose and lignin content between two different types of spectrometers. The model transfer effect of holocellulose content was better than that of lignin.
2. The stable consistent wavelengths screened by the SWCSS method can effectively reduce the differences between these two spectral instruments, and then the systematic errors that still exist after the SWCSS correction can be further corrected by the S/B method, and the predictive power of the spectral analysis model will be significantly improved.

3. The model transfer process using the SWCSS-S/B method involves fewer wavelength variables, reduces the dimensionality of the spectral matrix, and greatly improves the transfer efficiency.
4. Although the analysis object of this paper is only for the near infrared analysis model of holocellulose and lignin in pulp, the research methods and paths used are also instructive and applicable to other indicators of pulp materials, such as moisture and density, as well as to NIR analysis modeling in other industry sectors.

ACKNOWLEDGMENTS

This work was funded by the support of the Fundamental Research Funds of Research Institute of Forest New Technology, CAF(CAFYBB2019SY039).

REFERENCES CITED

- Abasi, S., Minaei, S., Jamshidi, B., Fathi, D., and Khoshtaghaza, M. H. (2019). "Rapid measurement of apple quality parameters using wavelet de-noising transform with Vis/NIR analysis," *Scientia Horticulturae* 252, 7-13. DOI: 10.1016/j.scienta.2019.02.085
- Bergman, E. L., Brage, H., Josefson, M., Svensson, O., and Sparén, A. (2006). "Transfer of NIR calibrations for pharmaceutical formulations between different instruments," *Journal of Pharmaceutical and Biomedical Analysis* 41(1), 89-98.
- Bin, J., Li, X., Fan, W., Zhou, J. H., and Wang, C. W. (2017). "Calibration transfer of near-infrared spectroscopy by canonical correlation analysis coupled with wavelet transform," *Analytist* 142(12), 2229-2238. DOI: 10.1039/c7an00280g
- Cao, X., Ding, H., Yang, L., Huang, J., Zeng, L., Tong, H., Su, L., Ji, X., Wu, M., and Yang, Y. (2022). "Near-infrared spectroscopy as a tool to assist *Sargassum fusiforme* quality grading: Harvest time discrimination and polyphenol prediction," *Postharvest Biology and Technology* 192, article no. 112030. DOI: 10.1016/J.POSTHARVBIO.2022.112030
- Du, W., Chen, Z. P., Zhong, L. J., Wang, S. X., Yu, R. Q., Nordon, A., and Holden, M. (2011). "Maintaining the predictive abilities of multivariate calibration models by spectral space transformation," *Analytica Chimica Acta* 690(1), 64-70. DOI: 10.1016/j.aca.2011.02.014
- Fatchurrahman, D., Nosrati, M., Amodio, M. L., Chaudhry, M. M. A., de Chiara, M. L. V., Mastrandrea, L., and Colelli, G. (2021). "Comparison performance of visible-NIR and near-infrared hyperspectral imaging for prediction of nutritional quality of goji berry," *Foods* 10(7), 1676. DOI: 10.3390/FOODS10071676
- Ferrara, G., Marcotuli, V., Didonna, A., Stellacci, A. M., Palasciano, M., and Mazzeo, A. (2022). "Ripeness prediction in table grape cultivars by using a portable NIR device," *Horticulturae* 8(7), 613. DOI: 10.3390/HORTICULTURAE8070613
- Feudale, R. N., Woody, N. A., Tan, H., Myles, A. J., Brown, S. D., and Ferré, J. (2002). "Transfer of multivariate calibration models: A review," *Chemometrics and Intelligent Laboratory Systems* 64(2), 181-192. DOI: 10.1016/S0169-7439(02)00085-0

- Hao, Y., Li, Z., Ding, N., Tang, X., and Zhang, C. (2022). "A new near-infrared fluorescence probe synthesized from IR-783 for detection and bioimaging of hydrogen peroxide in vitro and in vivo," *Spectrochimica Acta Part A: Molecular and Biomolecular Spectroscopy* 268, article no. 120642. DOI: 10.1016/J.SAA.2021.120642
- Haque, M. M., Uddin, M. N., Quaiyyum, M. A., Nayeem, J., Alam, M. Z., and Jahan, M. S. (2019). "Pulpwood quality of the second generation *Acacia auriculiformis*," *Journal of Bioresources and Bioproducts* 4(2), 73-79. DOI: 10.21967/jbb.v4i2.227
- Hasan, M. M., Chaudhry, M. M. A., Erkinbaev, C., Paliwal, J., Suman, S. P., and Rodas-Gonzalez, A. (2022). "Application of Vis-NIR and SWIR spectroscopy for the segregation of bison muscles based on their color stability," *Meat Science* 188, article no. 108774. DOI: 10.1016/J.MEATSCI.2022.108774
- Kang, W., Lin, H., Jiang, R., Yan, Y., Ahmad, W., Ouyang, Q., and Chen, Q. (2022). "Emerging applications of nano-optical sensors combined with near-infrared spectroscopy for detecting tea extract fermentation aroma under ultrasound-assisted sonication," *Ultrasonics Sonochemistry*, article no. 106095. DOI: 10.1016/J.ULTSONCH.2022.106095
- Li, L., Huang, W., Wang, Z., Liu, S., He, X., and Fan, S. (2022). "Calibration transfer between developed portable Vis/NIR devices for detection of soluble solids contents in apple," *Postharvest Biology and Technology* 183, article no. 111720. DOI: 10.1016/J.POSTHARVBIO.2021.111720
- Li, T., Liu, C., and Bit, L. (2018). "Study on near-infrared spectral model transfer of slope intercept correction algorithm on acid value and peroxide value of edible oil," *Chinese Journal of Cereals and Oils* 33(01), 118-124, 139.
- Liu, Y., Cai, W., and Shao, X. (2016). "Linear model correction: A method for transferring a near-infrared multivariate calibration model without standard samples," *Spectrochimica Acta Part A: Molecular and Biomolecular Spectroscopy* 169, 197-201. DOI: 10.1016/j.saa.2016.06.041
- Liu, Y., Xiong, Z., and Wang, Y. (2019a). "Model transfer study of lignin near-infrared spectral analysis between different models of portable spectrometers," *Journal of Forestry Engineering* 4(04), 93-98. DOI: 10.13360/j.issn.2096-1359.2019.04.014
- Liu, Y., Yang H., and Xiong, Z. (2019b). "Model transfer study of near-infrared analysis of lignin content in pulpwood," *Chinese Journal of Paper Making* 34(03), 43-49.
- Maraphum, K., Saengprachatanarug, K., Wongpichet, S., Phuphuphud, A., and Posom, J. (2022). "Achieving robustness across different ages and cultivars for an NIRS-PLSR model of fresh cassava root starch and dry matter content," *Computers and Electronics in Agriculture* 196, article no. 106872. DOI: 10.1016/J.COMPAG.2022.106872
- Moreira, S. A., Sarraguca, J., Saraiva, D. F., Carvalho, R., and Lopes, J. A. (2015). "Optimization of NIR spectroscopy based PLSR models for critical properties of vegetable oils used in biodiesel production," *Fuel* 150, 697-704. DOI: 10.1016/j.fuel.2015.02.082
- Ni, L., Han, M., Luan, S., and Zhang, L. (2019). "Screening wavelengths with consistent and stable signals to realize calibration model transfer of near infrared spectra," *Spectrochimica Acta Part A: Molecular and Biomolecular Spectroscopy* 206, 350-358. DOI: 10.1016/j.saa.2018.08.027
- Parrott, A. J., McIntyre, A. C., Holden, M., Colquhoun, G., Chen, Z. P., Littlejohn, D., and Nordon, A. (2022). "Calibration model transfer in mid-infrared process analysis

- with *in situ* attenuated total reflectance immersion probes,” *Analytical Methods* 14(19), 1889-1896. DOI: 10.1039/D2AY00116K
- Peng, J., Peng, S., Jiang, A., and Tan, J. (2011). “Near-infrared calibration transfer based on spectral regression,” *Spectrochimica Acta Part A: Molecular and Biomolecular Spectroscopy* 78(4), 1315-1320. DOI: 10.1016/j.saa.2011.01.004
- Poerio, D. V., and Brown, S. D. (2018). “Dual-domain calibration transfer using orthogonal projection,” *Applied Spectroscopy* 72(3), 378-391. DOI: 10.1177/0003702817724164
- Sadegaski, L. R., Myhre, K. G., and Delmau, L. H. (2022). “Multivariate chemometric methods and Vis-NIR spectrophotometry for monitoring plutonium-238 anion exchange column effluent in a radiochemical hot cell,” *Talanta Open*, article no. 100120. DOI: 10.1016/J.TALO.2022.100120
- Wang, A., Yang, P., Chen, J., Wu, Z., Jia, Y., Ma, C., and Zhan, X. (2019). “A new calibration model transferring strategy maintaining the predictive abilities of NIR multivariate calibration model applied in different batches process of extraction,” *Infrared Physics and Technology* 103, article no. 103046. DOI: 10.1016/j.infrared.2019.103046
- Pažitný, A., Boháček, Š., and Russ, A. (2011). “Application of distillery refuse in papermaking: Novel methods of treated distillery refuse spectral analysis,” *Wood Res.* 56(4), 533-544.
- Yu, Y., Huang, Y., Feng, W., Yang, M., Shao, B., Li, J., and Ye, F. (2021). “NIR-triggered upconversion nanoparticles@ thermo-sensitive liposome hybrid theranostic nanoplatform for controlled drug delivery,” *RSC Advances* 11(46), 29065-29072
- Zhang, L., Li, G., Sun, M., Li, H., Wang, Z., Li, Y., and Lin, L. (2017). “Kennard-Stone combined with least square support vector machine method for noncontact discriminating human blood species,” *Infrared Physics and Technology* 86, 116-119. DOI: 10.1016/j.infrared.2017.08.020
- Zhang, Y., Nock, J. F., Al Shoffe, Y., and Watkins, C. B. (2019). “Non-destructive prediction of soluble solids and dry matter contents in eight apple cultivars using near-infrared spectroscopy,” *Postharvest Biology and Technology* 151, 111-118. DOI: 10.1016/j.postharvbio.2019.01.009
- Zhang, L., Li, Y., Huang, W., Ni, L., and Ge, J. (2020). “The method of calibration model transfer by optimizing wavelength combinations based on consistent and stable spectral signals,” *Spectrochimica Acta Part A: Molecular and Biomolecular Spectroscopy* 227, 117647. DOI: 10.1016/j.saa.2019.117647
- Zhang, L., Wang, Y., Wei, Y., and An, D. (2022). “Near-infrared hyperspectral imaging technology combined with deep convolutional generative adversarial network to predict oil content of single maize kernel,” *Food Chemistry* 370, article no. 131047. DOI: 10.1016/J.FOODCHEM.2021.131047
- Zhao, Y., Yu, J., Shan, P., Zhao, Z., Jiang, X., and Gao, S. (2019). “PLS subspace-based calibration transfer for near-infrared spectroscopy quantitative analysis,” *Molecules* 24(7), article no. 1289. DOI: 10.3390/molecules24071289

Article submitted: August 3, 2022; Peer review completed: September 24, 2022; Revised version received and accepted: September 28, 2022; Published: October 3, 2022.
DOI: 10.15376/biores.17.4.6476-6489